Title

Identical oligomeric and fibrillar structures captured from the brains of R6/2 and knock-in mouse models of Huntington's disease.

Journal

Human molecular genetics, 19(1)

ISSN

0964-6906

Authors

Sathasivam, Kirupa
Lane, Amin
Legleiter, Justin
et al.

Publication Date

2010

DOI

10.1093/hmg/ddp467

Peer reviewed

Human Molecular Genetics, 2010, Vol. 19, No. 1 **65–78**
doi:10.1093/hmg/ddp467
Advance Access published on October 12, 2009

Identical oligomeric and fibrillar structures captured from the brains of R6/2 and knock-in mouse models of Huntington's disease

Kirupa Sathasivam[1], Amin Lane[2], Justin Legleiter[3], Alice Warley[4], Ben Woodman[1], Steve Finkbeiner[5,6], Paolo Paganetti[7], Paul J. Muchowski[3], Stuart Wilson[2] and Gillian P. Bates[1,*]

[1]Department of Medical and Molecular Genetics, King's College London School of Medicine, King's College London, 8th Floor Tower Wing, Guy's Tower, Great Maze Pond, London SE1 9RT, UK, [2]Microsens Biotechnologies, London Bioscience Innovation Centre, London NW1 0TU, UK, [3]Gladstone Institute for Neurological Disease and the Departments of Biochemistry and Biophysics of Neurology, University of California San Francisco, San Francisco, CA 94158, USA, [4]Centre for Ultrastructural Imaging, King's College London, London SE1 1UL, UK, [5]Taube-Koret Center for Huntington's Disease Research, Gladstone Institute of Neurological Disease, San Francisco, CA 94158, USA, [6]Departments of Neurology and Physiology, University of California, San Francisco, CA 94143, USA and [7]Neuroscience Discovery, Novartis Institutes for BioMedical Research (NIBR), Novartis Pharma AG, CH4002 Basel, Switzerland

Received August 19, 2009; Revised and Accepted October 5, 2009

Huntington's disease (HD) is a late-onset neurodegenerative disorder that is characterized neuropathologically by the presence of neuropil aggregates and nuclear inclusions. However, the profile of aggregate structures that are present in the brains of HD patients or of HD mouse models and the relative contribution of specific aggregate structures to disease pathogenesis is unknown. We have used the Seprion ligand to develop a highly sensitive enzyme-linked immunosorbent assay (ELISA)-based method for quantifying aggregated polyglutamine in tissues from HD mouse models. We used a combination of electron microscopy, atomic force microscopy (AFM) and sodium dodecyl sulphate–polyacrylamide gel electrophoresis (SDS–PAGE) to investigate the aggregate structures isolated by the ligand. We found that the oligomeric, proto-fibrillar and fibrillar aggregates extracted from the brains of R6/2 and *Hdh*Q150 knock-in mice were remarkably similar. Using AFM, we determined that the nanometre globular oligomers isolated from the brains of both mouse models have dimensions identical to those generated from recombinant huntingtin exon 1 proteins. Finally, antibodies that detect exon 1 Htt epitopes differentially recognize the ligand-captured material on SDS–PAGE gels. The Seprion-ligand ELISA provides an assay with good statistical power for use in preclinical pharmacodynamic therapeutic trials or to assess the effects of the genetic manipulation of potential therapeutic targets on aggregate load. This, together with the ability to identify a spectrum of aggregate species in HD mouse tissues, will contribute to our understanding of how these structures relate to the pathogenesis of HD and whether their formation can be manipulated for therapeutic benefit.

INTRODUCTION

Huntington's disease (HD) is an autosomal dominant late-onset neurodegenerative disorder with a mean age of onset of 40 years. Symptoms include psychiatric disturbances, motor disorders, cognitive decline and weight loss. Disease duration is 15–20 years and there are no effective disease-modifying treatments (1). The disease is caused by an expanded CAG trinucleotide repeat in the *HD* gene that is translated into a polyglutamine (polyQ) repeat in the

*To whom correspondence should be addressed. Tel: +44 2071883722; Fax: +44 2071882585; Email: gillian.bates@kcl.ac.uk

huntingtin (Htt) protein (2). Neuropathologically, HD is characterized by a generalized brain atrophy as well as neuronal cell loss in the striatum, cortex and other brain regions. Intracellular polyQ-containing aggregates are deposited throughout the neuropil and as inclusions in neuronal nuclei (3,4).

PolyQ aggregates formed *in vitro* from recombinant protein comprise a range of oligomeric, proto-fibrillar and fibrillar structures (5–7). However, it is not known whether these reflect the oligomeric polyQ structures that form *in vivo* in HD patients or in HD mouse models. Similarly, although the genetic and pharmacological manipulation of polyQ aggregates *in vitro* and in invertebrate disease models has suggested that either the prevention of aggregate formation or their partition into less toxic structures can have beneficial consequences (5,8–12), the role that polyQ aggregates play in disease pathology remains unclear. The ability to monitor the effects of aggregate manipulation in HD mouse models would help to determine the relevance of experiments performed in simple model systems. To this end, it is essential that the aggregate load in mouse tissues can be quantified and that the aggregate species that form *in vivo* can be identified.

We utilized two HD mouse models that were generated by very different approaches. The R6/2 mouse is transgenic for a human exon 1 Htt protein which in our colony has approximately 200Q (13). These mice develop an early-onset phenotype with rapid disease progression and as a consequence can realistically be used as a therapeutic screening tool (14). In our R6/2 colony, nuclear inclusions can be readily detected by immunohistochemistry in the cerebral cortex, striatum and hippocampus by 3 weeks of age (15,16), RotaRod impairment is apparent by 6 weeks and end-stage disease occurs at 15 weeks. The *Hdh*Q150 knock-in mouse is a more genetically precise model of the human disease, and carries approximately 150Q which has been inserted into the mouse *Hd* gene (*Hdh*) (17). In our $Hdh^{Q150/Q150}$ colony, nuclear inclusions were detected by immunohistochemistry in the striatum and hippocampus by 6 months and the cortex by 8 months (18), an impaired RotaRod performance was apparent by 18 months of age and end-stage disease occurs at around 22 months (18). The *Hdh*Q150 mice develop a phenotype that is remarkably similar to that found in R6/2 except that onset is much delayed and the disease progresses much more slowly over a period of 22 months (18,19). At the level of light microscopy, a complex distribution of aggregates in the form of nuclear inclusions and cytoplasmic aggregates are widely distributed throughout the brains of both models (18).

Quantification of the aggregate load in mouse tissues has primarily involved counting the number of striatal nuclear inclusions and measuring their diameter. However, this only samples a subset of the aggregate species in one small brain region and more quantitative approaches that are less work-intensive are desperately needed. We have previously used the filter retardation assay to detect aggregates in mouse tissues (20) but we have been unsuccessful in optimizing this as an *in vivo* screening tool owing to signal variability. However, even if these technical difficulties were overcome, this approach would still have the disadvantage of only measuring the presence of aggregates that are larger than the cellulose acetate membrane pore size and therefore retained on the membrane.

Here we describe the use of the Seprion ligand to establish an enzyme-linked immunosorbent assay (ELISA)-based method that provides a rapid, highly sensitive assay with good statistical power to detect changes in aggregate load in the brains of mouse models of HD. We demonstrate that the ligand captures a remarkably similar range of oligomeric, proto-fibrillar and fibrillar aggregates from the brains of both the R6/2 and *Hdh*Q50 mouse models and that these are comparable to those generated from recombinant proteins *in vitro*. Using atomic force microscopy (AFM) we show that the dimensions of nanometre globular aggregates from the R6/2 and *Hdh*Q150 knock-in brains are identical to those generated by the aggregation of recombinant exon1 Htt proteins containing just 46 and 53 polyQs. Finally, antibodies that detect exon 1 Htt epitopes differentially recognize the ligand-captured material on sodium dodecyl sulphate–polyacrylamide gel electrophoresis (SDS–PAGE) gels.

RESULTS

The Seprion ligand ELISA provides a highly quantitative assay for measuring polyQ aggregate load in Huntington's disease mouse tissue

The Seprion ligand has previously been used to isolate and quantify aggregated forms of the prion protein, Prp^{Sc} (21,22). It is a high molecular weight polymeric ligand that consists of repeating charged and hydrophobic chemical groups that interact with similar repeating groups that occur on aggregated proteins. The selectivity for aggregated proteins is based on the arrangement of large numbers of polar and hydrophobic regions in aggregated proteins which occur to a much lesser extent in a single unaggregated protein molecule.

We have used the Seprion ligand to develop an ELISA-based plate assay by which aggregated Htt is captured from tissue lysates and detected by immunoprobing with the S830 antibody that was raised against the N-terminal exon 1 Htt protein (23). We quantified the aggregate load in each of the five brain regions from female R6/2 mice at 2, 4, 6, 8 and 12 weeks of age. The Seprion ligand extracted statistically significant levels of aggregates from the striatum and hippocampus at 2 weeks of age, the cerebral cortex and brain stem at 4 weeks and cerebellum at 6 weeks (Fig. 1A). Only signals corresponding to background levels were measured in wild-type (WT) samples, equivalent to those obtained with capture-buffer only controls. The ELISA readings have proved to be highly reproducible between experiments, e.g. there was no difference in the aggregate load measured in the cortex from four different series of 12-week-old R6/2 mice using different batches of ligand-coated plates over a period of 2 years ($F_{(3,21)} = 2.121$, $P = 0.133$). We have previously shown that nuclear inclusions form in a number of R6/2 peripheral tissues (24). We applied the Seprion ELISA to quantify the corresponding aggregate levels and found that statistically significant amounts could be detected by 8 weeks in muscle and by 12 weeks in pancreas and liver (Fig. 1B). Therefore, the Seprion ELISA might provide a highly sensitive method of quantifying the level of aggregated polyQ in tissues from mouse models of HD. This assay has great potential for use as an outcome measure either in

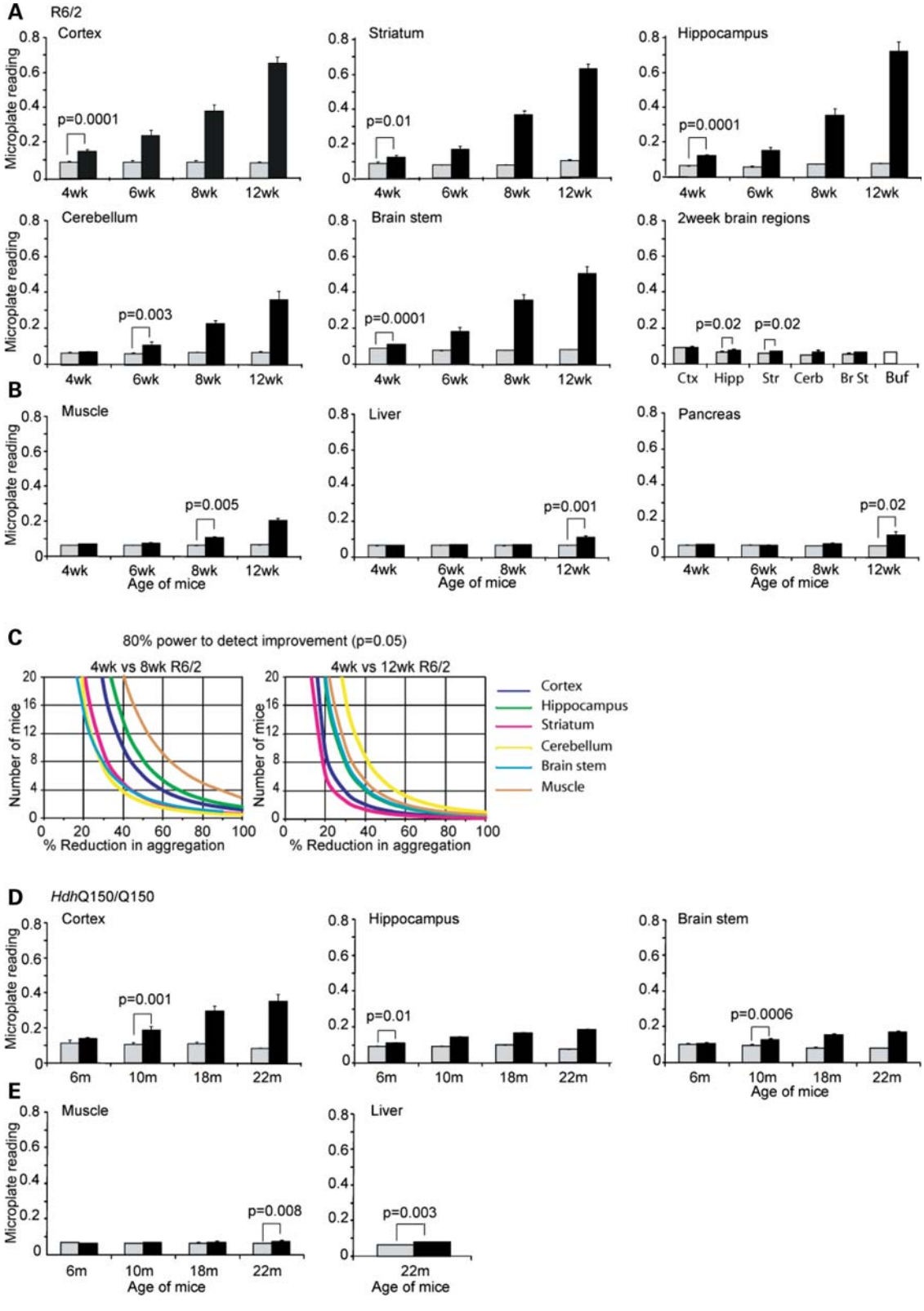

Figure 1. Seprion ligand quantification of aggregate load in tissues from HD mouse models. Quantification of aggregate levels in brain regions (**A**) and peripheral tissues (**B**) of R6/2 mice. (**C**) Power analysis indicating the number of R6/2 mice required to have an 80% chance of detecting a specific percentage reduction in aggregate load in response to a therapeutic intervention initiated at 4 weeks of age and terminated at either 8 weeks or 12 weeks of age ($P > 0.05$). Quantification of aggregate levels in brain regions (**D**) and peripheral tissues (**E**) of $Hdh^{Q150/Q150}$ mice. In all cases, $n = 6$/genotype/age and the age at which statistically significant aggregate levels can first be detected is indicated by the corresponding P-value. Black bars = R6/2 or *Hdh*Q150, gray bars = wild-type. Ctx = cerebral cortex; Hipp = hippocampus; Str = striatum; Cerb = cerebellum; Br St = brain stem; Buf = buffer.

preclinical efficacy trials to test the effect of potential therapeutic interventions or in mice with genetic modifications that might modulate HD-related mouse phenotypes. For example, for the purpose of a pharmacodynamic trial in which a compound has been administered to R6/2 mice from 4 to 8 weeks of age, power calculations (25) indicate that as few as eight mice would be sufficient to give an 80% chance of detecting a 30–50% reduction in aggregate load in brain regions ($P < 0.05$; Fig. 1C).

The aggregate pathology in the R6/2 mice occurs throughout the brain and in many peripheral tissues. We had assumed that this widespread distribution occurred because they express a small N-terminal fragment of mutant Htt. Therefore, we were surprised to find that at end-stage disease, polyQ aggregates in the form of nuclear inclusions and cytoplasmic aggregates are present in all brain regions of homozygous *Hdh*$^{Q150/Q150}$ knock-in mice (18). Similarly, we have recently demonstrated that the distribution of polyQ aggregates throughout the peripheral tissues of 12–14 week R6/2 mice and 22 month *Hdh*Q150 knock-in mice is almost identical (H. Moffitt, G. McPhail, B. Woodman, C. Hobbs and G. Bates, manuscript in preparation) suggesting that HD pathology may not be restricted to the CNS in HD patients. Therefore, we applied the Seprion ELISA to measure the level of polyQ aggregation that had accumulated in the cerebral cortex, hippocampus and brain stem from *Hdh*$^{Q150/Q150}$ mice aged 6, 10, 18 and 22 months (Fig. 1D). The striata and cerebella from this series of tissues had been used for RNA analyses (18). As with the R6/2 mice, statistically significant levels were present in the hippocampus (6 months) before the cortex and brain stem (10 months). These ages correspond to those at which inclusions are apparent in the brain by light microscopy (18). In the periphery, statistically significant levels of aggregates could be detected in muscle and liver at 22 months (Fig. 1E). The microplate readings were lower for the *Hdh*$^{Q150/Q150}$ tissues than for the R6/2 tissues. However, the difference in these values does not necessary reflect differences in the levels of aggregates that have accumulated in the tissues of the two models. The S830 antibody has a different affinity to the mutated versions of human Htt (in the R6/2 mouse) and mouse Htt (in the *Hdh*Q150 knock-in mice).

Immuno-EM reveals diverse oligomeric and fibrillar Htt species in brain tissue from Huntington's disease mouse models

We employed immuno-electron microscopy (EM) to investigate the morphology of the ligand-isolated aggregated Htt species. Aggregates were captured from cortical lysates by Seprion ligand-coated magnetic beads and eluted onto EM grids, processed for transmission EM and immunoprobed with gold-labelled MW8 (26), MW1 (26) or 3B5H10 (27). Bead capture was performed on cortices from R6/2 mice aged 2, 4, 6 and 12 weeks and from *Hdh*$^{Q150/Q150}$ mice aged 2, 3, 4 and 22 months as well as on the cortices of matched WT littermates at each time point. The number of mice examined is summarized in Table 1. While in the case of R6/2 mice, we chose time points that span the course of the disease, for the *Hdh*$^{Q150/Q150}$ we instead focussed on young mice, asking how soon aggregate structures can be detected, but also included mice at end-stage disease for comparison with late-stage R6/2. *Hdh*$^{Q150/Q150}$ mice aged 2, 3 and 4 months would all correspond to R6/2 mice of less than 4 weeks of age with respect to the stage of disease.

Table 1. Number of R6/2 and wild-type (WT) mice used for the electron microscopy and SDS–PAGE analyses

Age (weeks)	R6/2	WT	Age (months)	Hdh$^{Q150/Q150}$	WT
2	8	4	2	3	1
4	8	4	3	2	1
6	7	3	4	2	1
12	11	6	22	2	1

Immunolabelling of bead captured and eluted cortical aggregates from both R6/2 and *Hdh*$^{Q150/Q150}$ cortices with MW8 consistently identified fibrillar structures. The fibrils captured from the R6/2 series of tissues increased in both amount and size as a function of disease progression and could be detected as early as 2 weeks of age (Fig. 2A). In the case of the *Hdh*$^{Q150/Q150}$ knock-in mice, fibrils were prominent at 22 months and were isolated from the cortex of mice as young as 2 months (Fig. 2B). The antibodies MW1 and 3B5H10 detected a variety of small aggregate structures including oligomers and protofibrils in both mouse models (Fig. 2A and B). The complete spectrum of captured aggregate structures, the age of mouse from which each was isolated, and the antibodies with which they were detected is summarized in Figure 3. The Seprion ligand captured a range of oligomeric/proto-fibrillar (Fig. 3B–E) and fibrillar (Fig. 3F–I) structures. Large filamentous aggregates have frequently been generated from polyQ peptides (28,29) and exon 1 Htt proteins (6,7,30,31) *in vitro* and visualized by EM. In one case, EM has been used to describe fibrillar structures purified from the brains of an inducible HD mouse model by gradient fractionation (32). The filamentous/fibrillar aggregates isolated by the Seprion ligand (Fig. 3F–I were in all cases recognized by MW8, but MW1 and 3B5H10 epitopes were only present on the smaller, immature fibrils (Fig. 3F).

The structures illustrated in Figure 3A–E have not previously been isolated from *in vivo* tissues. Those shown in panels A–D were captured from both R6/2 and *Hdh*$^{Q150/Q150}$ brains, whereas the proto-fibrillar bundles illustrated in (E) were only observed in material extracted from *Hdh*$^{Q150/Q150}$ knock-in mice. The immunolabelled shadows depicted in Figure 3A were captured from R6/2 and *Hdh*$^{Q150/Q150}$brains, were detected with both MW1 and 3B5H10 and never seen in the material captured from WT mice. However, whether they represent an aggregated form of the protein is not clear. The structures shown in Figure 3B and C have been formed by *in vitro* aggregation of 44Q exon 1 Htt (6), of a truncated 30Q exon 1 protein (7), polyQ peptides (28) and of Aβ42 (30) and termed oligomers (6,30) and oligomers/protofibrils (7). Those illustrated in Figure 3D and E have been generated *in vitro* from 44Q exon 1 Htt (6), and the truncated 30Q exon 1 protein (7) and termed oligomers and protofibrils. We used electron tomography to reveal the three-dimensional structure of the protofibrillar bundles in Figure 3D (Fig. 4A) and the thin filaments in Figure 3G (Fig. 4B). Figure 4 presents still images of the

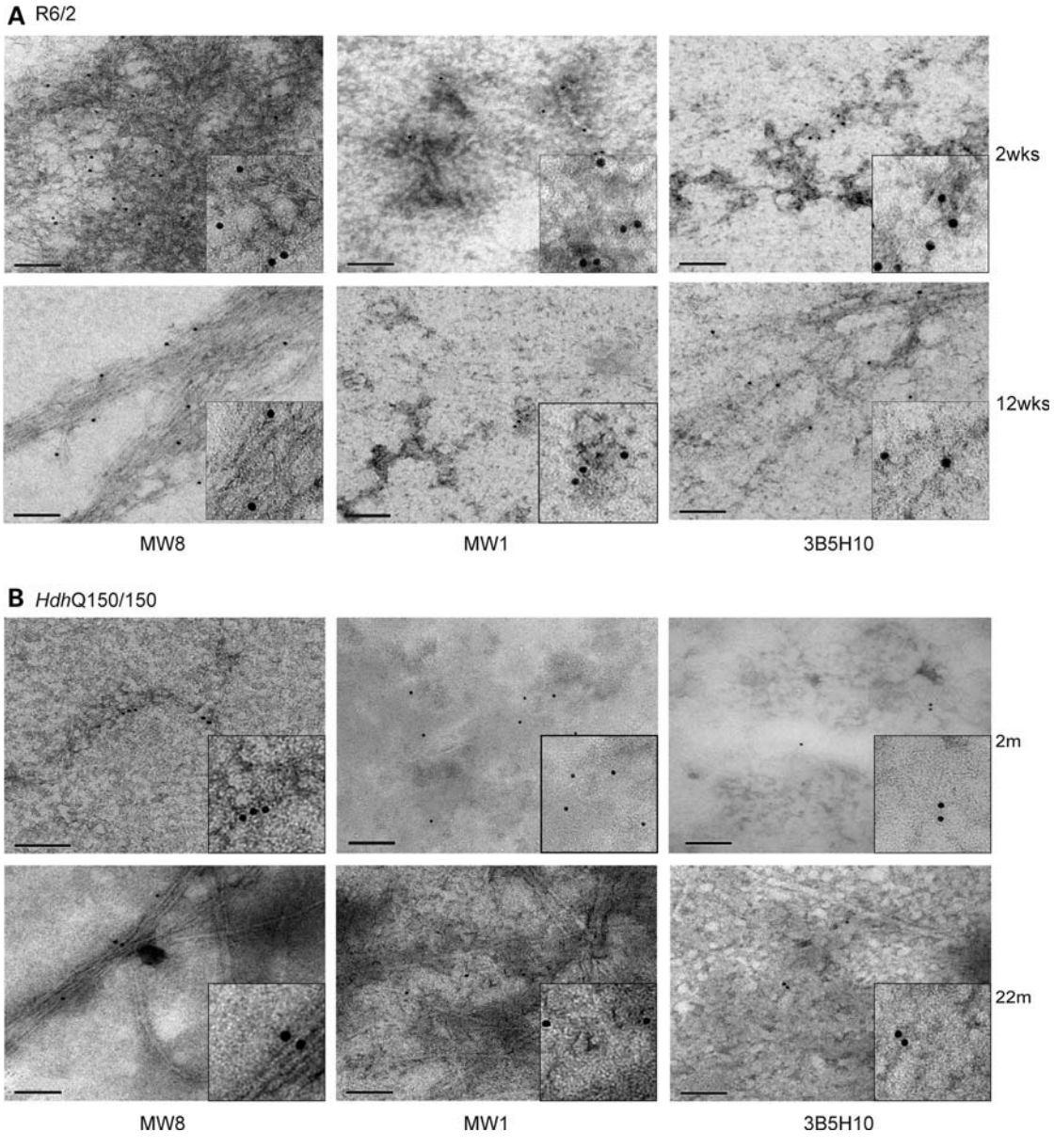

Figure 2. Immuno-EM analysis of captured material from R6/2 and $Hdh^{Q150/Q150}$ cortex. Representative examples of immunogold labelling of Htt aggregates with MW8, MW1 and 3B5H10 captured from the cortex of (**A**) R6/2 mice aged 2 and 12 weeks of age and (**B**) $Hdh^{Q150/Q150}$ mice aged 2 and 22 months of age. MW8 immunolabels fibrillar structures at each age in both the R6/2 and $Hdh^{Q150/Q150}$ tissue. Oligomers and protofibrils (A) and oligomers (B) detected by MW1 and protofibrils (A) and oligomers (B) detected by 3B5H10 are shown. Scale bar = 100 nm.

three-dimensional structures shown in the movies in Supplementary Material, Figure S1.

Globular nanometre oligomers isolated from the R6/2 and $Hdh^{Q150/Q150}$ mouse brains have identical dimensions as those generated from exon 1 Htt proteins *in vitro*

We applied AFM to provide a more quantitative comparison of the oligomeric aggregates that were captured by the Seprion ligand. We discovered empirically that elution with 100 mM KCl (as described in the Materials and Methods) differentially eluted globular nanometre oligomers, while other aggregate species remained bound to the ligand. We used western blotting to demonstrate that the eluted material was an oligomeric form of Htt (Supplementary Material, Figure S2). The globular oligomers appeared to be very similar to those that had been previously generated *in vitro* (5,6,31) and, therefore, we focussed our AFM analysis on the quantification of these structures rather than on fibrillar structures which we had identified and characterized extensively by EM (Figures 2 and 3). Globular oligomers were captured from cortical tissue from R6/2 mice aged 2, 4, 6 and 12 weeks ($n = 2$/per age), from $Hdh^{Q150/Q150}$ aged 2, 3, 8 and 22 months ($n = 2$/age) and from matched WT controls. Particles of approximately 20–40 nm in diameter were eluted from ligand-coated beads from both R6/2 and $Hdh^{Q150/Q150}$ brains

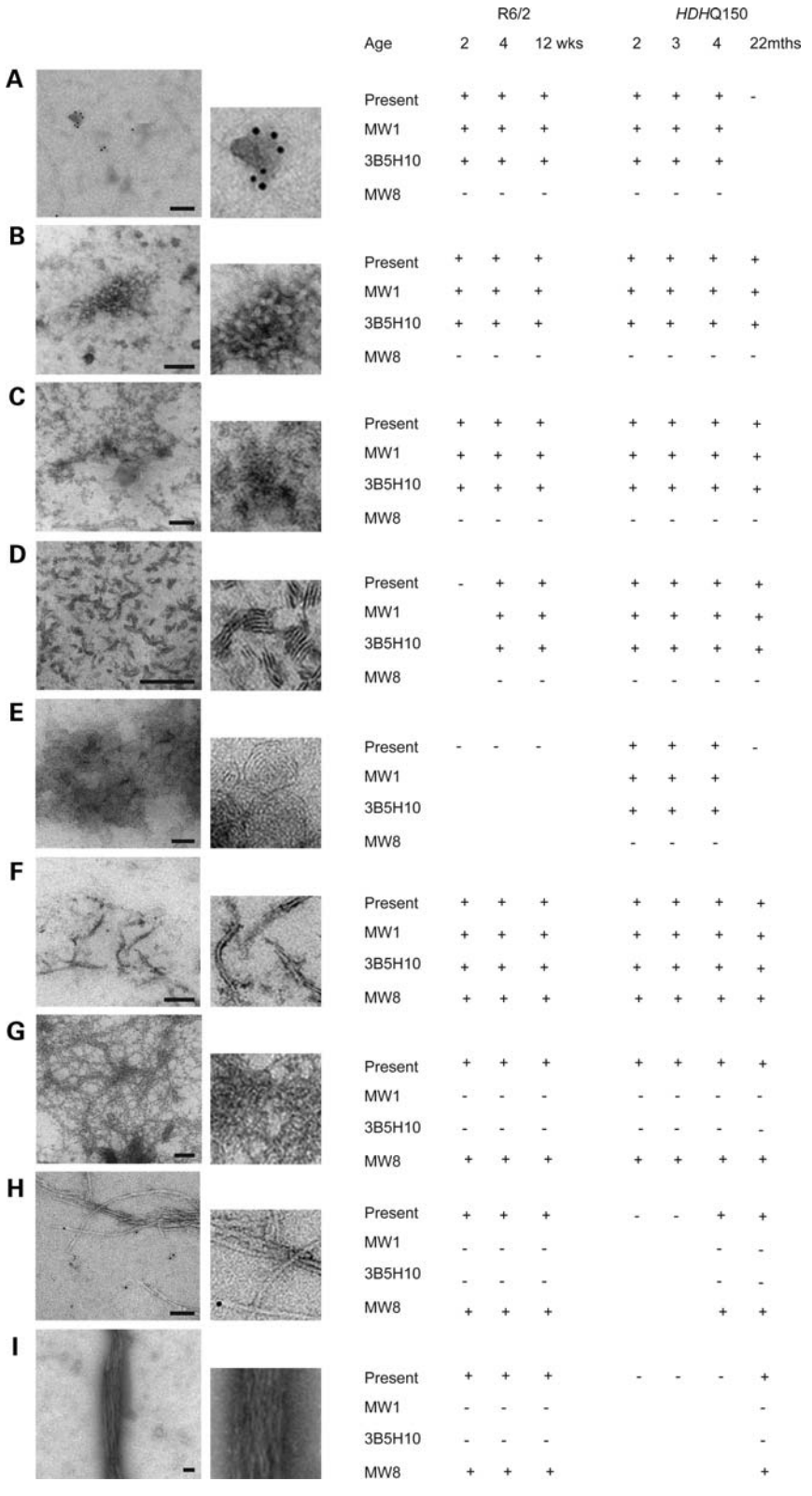

Figure 3. Variation in the oligomeric and fibrillar structures isolated from R6/2 and *Hdh*$^{Q150/Q150}$ brains before phenotype onset and at late-stage disease. (**A**) Immunolabelled 'shadows', (**B**–**E**) oligomeric/proto-fibrillar structures and (**F**–**I**) immature fibrils and fibrillar structures that have been consistently captured by the Seprion ligand bead-captured material as identified by transmission EM and immunogold-labelling. The right-hand table indicates the age at which a structure was identified in each of the mouse models and if present, whether it was associated with immunogold labelling with MW1, 3B5H10 or MW8. Scale bar = 100 nm.

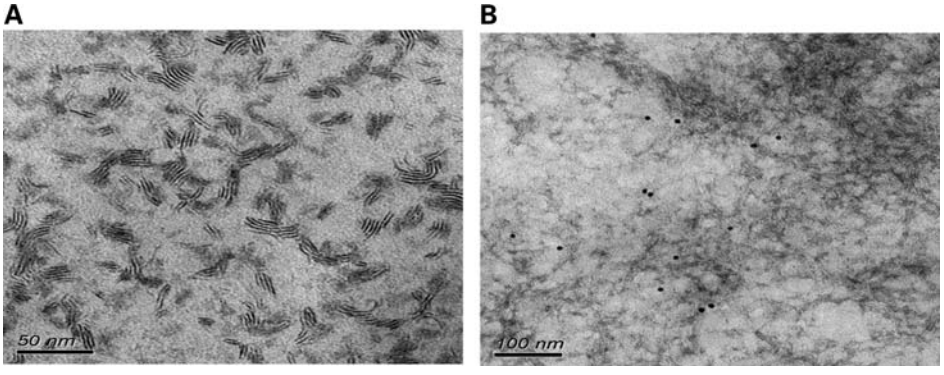

Figure 4. Still images of the electron tomography of oligomeric/proto-fibrillar structures captured from R6/2 and *Hdh*$^{Q150/Q150}$ brains for which the three-dimensional structure is shown in Supplementary Material, Figure S1. (**A**) Electron tomography of oligomeric structures illustrated in Figure 3D and **B** of the filamentous structures illustrated in Figure 3G immunolabelled with MW8.

at all ages tested (Fig. 5A). No oligomeric structures were eluted from WT tissue. For comparison, oligomers were generated *in vitro* by the aggregation of 2 μM recombinant exon 1 Htt proteins with either 53Q or 46Q for 1 h (Fig. 5A). It was striking that the dimensions of the globular oligomers that were eluted from ligand-captured material from both R6/2 and *Hdh*$^{Q150/Q150}$ tissue was found to be identical to those generated from the incubation of the recombinant exon 1 Htt proteins *in vitro* (Fig. 5B).

The Seprion ligand captures Htt species that resolve as monomers on SDS–PAGE

We employed SDS–PAGE to investigate the detergent-soluble properties of the mutant Htt species that were eluted from the Seprion ligand after capture from cortical lysates using ligand-coated magnetic beads. Eluted material from R6/2 mice aged 2, 4, 6 and 12 weeks of age was fractionated by SDS–PAGE alongside age-matched tissue lysates and immunoprobed with a series of antibodies: S830, MW1, MW8 and 3B5H10 (Fig. 6). In tissue lysates, all four antibodies detected the soluble R6/2 transprotein monomer that became less intense with age because of its sequestration into polyQ aggregates. The migration of the transprotein varied between lysates because the CAG repeat is unstable on transmission and therefore the polyQ repeat length differed between mice. Although an exon 1 Htt protein that carries a polyQ repeat of approximately 200Q is approximately 30 kDa in size, its migration by SDS–PAGE was retarded to approximately 80 kDa by the polyQ tract. Both S830 and 3B5H10 (Fig. 6A, D, E and F), and in some cases MW1 (Fig. 6C), detected a high molecular weight fragment in cortical lysates that migrated at the top of the resolving gel and rapidly diminished with age (as indicated by asterisk). MW1 detected the soluble transprotein in 4 and 6 week lysates and at 12 weeks, in most experiments, it detected a doublet above which there is a smear overlaying a ladder of fragments (Fig. 6G). From 6 weeks of age onwards, S830 and MW8 (Fig. 6A and B), but not MW1 or 3B5H10, detected detergent-insoluble aggregates that were retained in the stacking gel.

After bead-capture and SDS–PAGE, S830 and MW8 only detected the detergent-insoluble aggregates in the stacking gel, indicating that the soluble protein had not been extracted by the Seprion ligand (Fig. 6A and B). In contrast, MW1 and 3B5H10 detected fragments in the bead-captured material that resolved at a similar size to the soluble transprotein, but that were not detected by either S830 or MW8 (Fig. 6C–G). In material captured from the same lysates, MW1 and 3B5H10 produced comparable signals on western blots (Fig. 6C–E). The signals obtained with MW1 were always prominent in lysates from 4-week-old mice (>15 separate experiments). However, the ligand captured Htt species that resolve as a soluble monomer were not only seen at younger ages and were also captured from lysates of 6, 8 or 12 week R6/2 mice as detected by 3B5H10 (Fig. 6F). These fragments were never detected with S830 or MW8. The consistency of the MW1 results make it unlikely that an interaction between soluble exon 1 Htt and the ligand is causing the exon 1 protein to adopt a structure (retained upon SDS–PAGE), as if that were the case, there would be no reason to expect their detection to be disease-stage specific. Instead, the Seprion ligand has extracted either aggregated Htt species or misfolded monomers, which upon SDS–PAGE exhibited a comparable migration to that of the soluble monomer but are differentially recognized by antibodies that detect the exon 1 Htt protein.

DISCUSSION

We have shown that the Seprion ligand can be used to isolate and characterize aggregated Htt species that form in mouse models of HD. Using EM and AFM we have demonstrated that the brains of both the R6/2 and *Hdh*Q150 knock-in mouse models contain a diverse and comparable range of Htt aggregate structures. The oligomeric and fibrillar aggregates that were captured by the Seprion ligand were remarkably similar to those that have previously been generated through the aggregation of exon 1 Htt proteins *in vitro* (5,7,33,34). This similarity was particularly striking in the case of our AFM analysis where the dimensions of the nanometre globular oligomers isolated from the R6/2 and *Hdh*$^{Q150/Q150}$ brains were practically identical to those generated from recombinant exon 1 Htt *in vitro*. This finding was unexpected given that *Hdh*Q150 knock-in mice express full-length mouse Htt with approximately 150Q, R6/2 mice

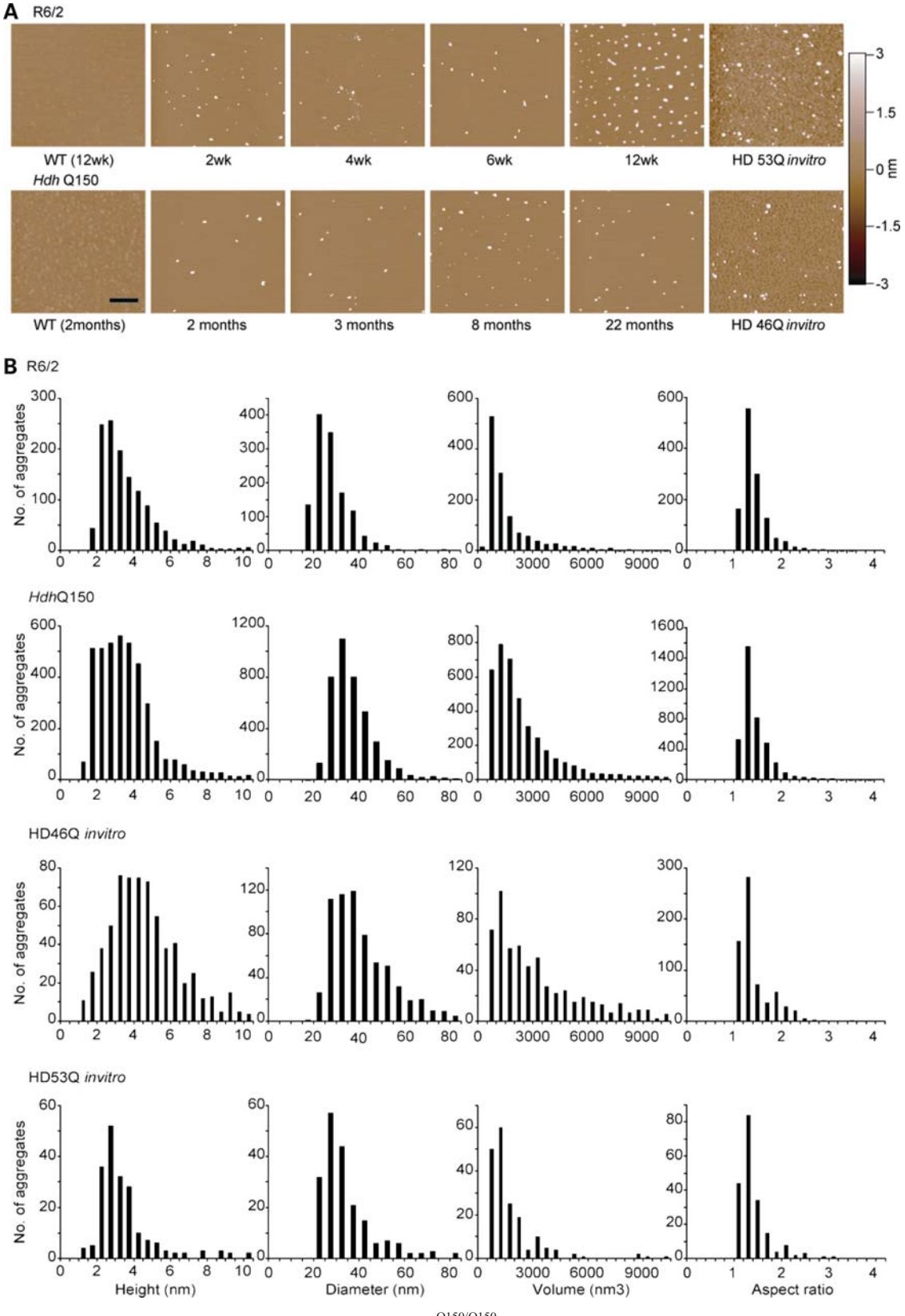

Figure 5. AFM analysis of nanometre globular aggregates from R6/2 and $Hdh^{Q150/Q150}$ brains. (**A**) AFM of Seprion ligand-captured material from both R6/2 and $Hdh^{Q150/Q150}$ cortex at the ages indicated fractionated to resolve nanometre globular oligomers. Observed aggregates were similar to those generated by the *in vitro* incubation of exon 1 Htt proteins with 53Q or 46Q at 2 μM for 1 h. Scale bar = 400 nm. (**B**) Histograms collating the height, diameter, volume and aspect ratio (longest width/shortest width) of the R6/2 and $Hdh^{Q150/Q150}$ aggregates measured at all ages. There is a remarkable similarity in the dimensions of the aggregates isolated from the R6/2 and $Hdh^{Q150/Q150}$ mice. These are comparable to those generated by the aggregation of 2 μM exon 1 Htt proteins with 53Q or 46Q *in vitro* for 1 h.

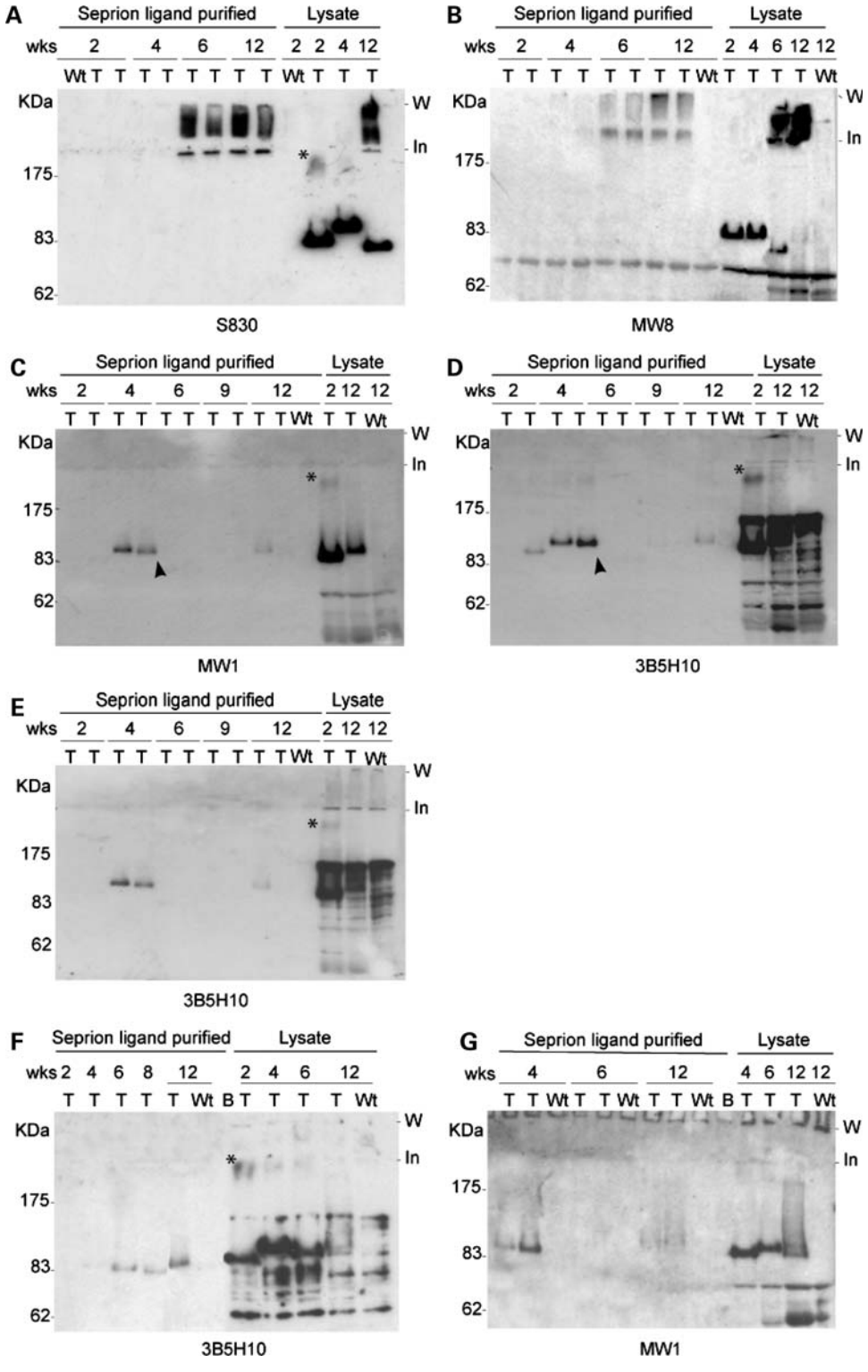

Figure 6. SDS–PAGE and immunoblotting of Seprion bead-captured aggregates from R6/2 cortex. Seprion ligand bead-captured material was fractionated by 10% SDS–PAGE alongside the corresponding mouse lysates. Blots were immunoprobed with S830 (**A**), MW8 (**B**), MW1 (**C,G**) or 3B5H10 (**D–F**) antibodies. In (C) and (D) material had been captured from the same lysates, fractionated on two gels and subsequently immunoprobed with MW1 (C) and 3B5H10 (D). The blot in (C) was stripped and reprobed with 3B5H10 (F). Asterisks denote high molecular bands detected by S830, 3B5H10 and MW1 that enter the resolving gel. Arrows indicate fragments that resolve at a size similar to monomeric Htt that are differentially recognized by the Htt antibodies. T = R6/2 transgenic; Wt = wild-type; B = buffer; W = well; In = interface between the stacking and resolving gel.

express a human exon 1 Htt transgene with approximately 200Q and the recombinant proteins were human exon 1 Htt with 46Q and 53Q. However, this observation is in keeping with our recent demonstration that the smallest N-terminal fragment generated from full-length Htt in the *Hdh*Q150 knock-in mice is an exon 1 Htt protein (C. Landles, K. Sathasivam, A. Weiss, B. Woodman, H. Moffitt, S. Finkbeiner, B. Sun, J. Gafni, L. Ellerby, Y. Trottier, W. Richards, A. Osmand, P. Paganetti and G. Bates, manuscript in preparation), and demonstrates that the wide variation in polyQ length carried by these exon 1 proteins does not have a detectable impact on the dimensions of the globular oligomers.

We extracted a diverse spectrum of oligomeric and fibrillar structures from the brains of both the R6/2 and *Hdh*Q150 mouse models. In the case of R6/2, we analysed brain tissue from mice aged 2, 4, 6 and 12 weeks of age, spanning the course of disease from a presymptomatic state to pronounced symptomatology. The entire spectrum of aggregate species was extracted from the brain tissue at each of these ages. However, the amount of fibrillar material increased considerably with disease progression to the extent that the EM grids were covered in fibrils from R6/2 mice at 12 weeks and $Hdh^{Q150/Q150}$ mice at 22 months. At late-stage disease the high density of fibrillar aggregates most likely masked the presence of oligomeric and proto-fibrillar structures making it difficult to assess their relative contributions. Our analysis of $Hdh^{Q150/Q150}$ mice focussed on very early time-points (2, 3 and 4 months), all of which precede overt symptomatology by several months, as we were interested in determining how early aggregated structures can be identified in these mice. Surprisingly, we were able to extract aggregate structures from $Hdh^{Q150/Q150}$ brains as early as 2 months of age.

Fibrillar aggregates have previously been imaged in tissue sections from HD post-mortem brains and HD mouse models (3,15,35) by EM, and therefore, we can be confident that the fibrillar structures that we have extracted from tissue sections exist *in vivo*. However, without being able to image mutant Htt oligomers and proto-fibrils in tissue sections, we cannot be certain that the aggregates isolated by the Seprion ligand have the same structure as those that form *in vivo*. To address this, we propose that the complexity of the aggregate structures that have been isolated, and the consistent variability in their relative proportions at different stages of disease, make it extremely unlikely that they have been generated through an interaction between the ligand and the soluble mutant Htt protein. In addition, as well as being very comparable to those that have been generated *in vitro* from exon 1 mutant Htt constructs they are also remarkably similar to those formed by other amyloidogenic proteins that have been studied in detail (36–39).

In this study, we used a panel of antibodies that recognize epitopes within the exon 1 Htt protein: MW8, MW1, 3B5H10 and S830. In all cases, these antibodies recognize a subset of exon 1 Htt structures. S830 is our in-house sheep polyclonal antibody that was raised against an exon 1 Htt recombinant protein with 53Q (23). We routinely use this antibody for western blots, on which it detects an exon 1 Htt monomer and the detergent-insoluble aggregated Htt that is retained in the stacking gel. We also use S830 for the detection of intranuclear inclusions and cytoplasmic aggregates by immunohistochemistry. MW8 also detects both the soluble exon 1 Htt monomer and detergent-insoluble aggregated forms on western blots. It is raised against an epitope at the C-terminus of exon 1 Htt and we have recently shown that although MW8 can be used to immunoprecipitate full-length Htt and all N-terminal proteolytic fragments thereof, if used to probe western blots, it behaves as a C-terminal exon 1 Htt neo-epitope antibody. On western blot, it only detects an exon 1 Htt protein and does not detect the C-terminus of exon 1 if it is embedded in a larger fragment of Htt (C. Landles, K. Sathasivam, A. Weiss, B. Woodman, H. Moffitt, S. Finkbeiner, B. Sun, J. Gafni, L. Ellerby, Y. Trottier, W. Richards, A. Osmand, P. Paganetti and G. Bates, manuscript in preparation). This suggests that MW8 is sensitive to the conformation of this epitope. In this study, MW8 detected monomeric Htt and detergent-insoluble aggregates on western blots as would be predicted. When immunogold labelled and used for EM, MW8 detected the fibrillar but, surprisingly, not oligomeric Htt that had been extracted from R6/2 brains. It would be surprising if the epitope had been cleaved or processed in oligomers, but not in fibrils and therefore the failure to detect oligomeric structures is more likely owing to the fact that the epitope has become inaccessible to MW8 or has adopted a conformation not recognized by MW8.

The monoclonal antibodies MW1 and 3B5H10 both recognize an expanded polyQ tract. It is known that the MW1 epitope is rapidly lost upon aggregation (10) and MW1 has been proposed to bind polyQ in a linear lattice model (40). Consistent with this, we found that MW1 and 3B5H10 did not recognize the detergent-insoluble aggregated material that is retained in the stacking gel on western blots and failed to detect fibrillar structures by immuno-EM. We performed SDS–PAGE and western blot analysis to examine the detergent solubility of the Seprion ligand material that had been captured from R6/2 mouse brains at different stages of disease. We had expected that the captured material would be retained in the stacking gel as was observed by immunoprobing with S830 and MW8. Unexpectedly, MW1 and 3B5H10 identified exon 1 Htt fragments with a comparable migration to the soluble monomer which were predominantly detected in lysates of brain tissue from R6/2 mice at 4 weeks of age. Both antibodies recognize the polyQ tract. A crystal structure of MW1 bound to polyQ showed that polyQ can adopt an extended coil-like structure (41) and an independent study demonstrates that 3B5H10 binds to a compact β-sheet-like structure of polyQ in a monomeric Htt fragment (M. Arrasate, J. Miller, E. Brooks, C. Peters-Libeu, J. Legleiter, D. Hatters, J, Curtis, K. Cheung, P. Krtishnan, S. Mitra, K. Widjaja, B. Shaby, Y. Newhouse, G. Lotz, V. Thulasiramin, F. Saudou, P. Muchowski, M. Segal, K. Weisgraber and S. Finkbeiner, manuscript in preparation). The Seprion ligand appears to extract structures from R6/2 brains that are detergent-soluble and are recognized by MW1 and 3B5H10 when fractionated by SDS–PAGE. It is not clear why these fragments are not detected by S830 and MW8, especially by S830, which gives very strong signals on western blots of brain lysates.

We have developed a highly quantitative ELISA-based assay for measuring the aggregate load in tissues from mouse models of HD with good statistical power. This has

provided us with a rapid and sensitive pharmacodynamic read-out for the preclinical assessment of therapeutic approaches predicted to modify Htt aggregation. This assay can also be used to determine whether specific genetic manipulations can modify Htt aggregation and other mouse HD-related phenotypes, thereby facilitating a preclinical validation of potential therapeutic targets. This can be complemented with agarose gel electrophoresis for resolving aggregates (AGERA), an agarose gel-based method that has the potential to detect overall changes in aggregate size distribution (42). Chemical compounds and molecular chaperones that partition aggregates into less toxic species *in vitro* have been identified (5,10,30). Our ability to quantify the aggregate load in the tissues from HD mouse models and to identify a range of aggregate structures that form *in vivo* will be essential in validating the therapeutic potential of these approaches.

MATERIALS AND METHODS

Huntington's disease mouse models

Hemizygous R6/2 mice (13) were bred by backcrossing R6/2 males to (CBA × C57Bl/6) F1 females (B6CBAF1/OlaHsd, Harlan Olac, Bicester, UK). *Hdh*$^{Q150/Q150}$ homozygous knock-in mice (17,18) on a (CBA × C57Bl/6) F1 background were generated by intercrossing *Hdh*$^{Q150/Q7}$ heterozygous CBA/Ca and C57BL/6J congenic lines (inbred lines from Harlan Olac, Bicester, UK). All the animals were subject to a 12 h light/dark cycle and had unlimited access to water and breeding chow (Special Diet Services, Witham, UK). Housing conditions and environmental enrichment were as previously described (25). R6/2 mice were always housed with WT mice. The CAG repeat size in the R6/2 mice was 202.6 ± 4.7 and in the *Hdh*Q150 mice was 155.8 ± 1.0 (SD).

Genotyping and CAG repeat sizing

R6/2 and *Hdh*$^{Q150/Q150}$ mice were identified by polymerase chain reaction of tail-tip DNA. For R6/2, a 10 μl reaction contained 100 ng DNA, 1 × Thermo-Start master mix (Thermo Scientific), 1 μl DMSO, 10 ng/μl forward primer 33727 [5′-CGCAGGCTAGGGCTGTCAATCATGCT-3′] and 10 ng/μl reverse primer 32252 [5′-TCATCAGCTTTTCCAGGGTC GCCAT-3′]. Cycling conditions were: 15 min at 94°C, 35 × (30 s at 94°C; 30 s at 60°C, 60 s at 72°C) and 10 min at 72°C. The amplified R6/2 transgene product was 272 bp. For *Hdh*Q150 mice, a 20 μl reaction contained 150 ng tail-tip DNA, 0.1 mM dNTPs, 2 M betaine (Sigma), 1× Detloff buffer [15 mM Tris–HCl (pH 8.8), 15 mM Tris–HCl (pH 9.0), 16 mM $(NH_4)_2SO_4$, 2.5 mM $MgCl_2$, 0.15 mg/ml bovine serum albumin (BSA), 0.007% β-mercaptoethanol], 10 ng/μl forward primer MHD16 [5′-CCCATTCATTGCCTTGCTGC TAGG-3′], 10 ng/μl reverse primer MHD18 [5′-GACTCAC GGTCGGTGCAGCGGTTCC-3′] and 1 U Herculase *Taq* polymerase (Stratagene). Amplification conditions were: 5 min at 95°C, 30 × (30 s at 94°C, 30 s at 58°C, 3 min at 72°C) and 5 min at 72°C. The WT allele amplified a 278 bp product, whereas the *Hdh*Q150 knock-in allele amplified an approximately 707 bp product. Amplification of the CAG repeat from R6/2 mouse DNA was performed with a FAM-labelled forward primer (GAGTCCCTCAAGTCCTTCC AGCA) and reverse primer (GCCCAAACTCACGGTCGGT) in 10 μl reactions containing: 0.2 mM dNTPs; 10% DMSO; AM buffer (67 mM Tris–HCl pH 8.8; 16.6 mM $(NH_4)SO_4$; 2 mM $MgCl_2$; 0.17 mg/ml BSA) and 0.5 U AmpliTaq DNA polymerase (Applied Biosystems). Cycling conditions were: 90 s at 94°C, 24 × (30 s at 94°C; 30 s at 65°C; 90 s at 72°C) and 10 min at 72°C. For *Hdh*Q150 mice, the amplification reaction was as for genotyping (above) with a FAM-labelled reverse MHD18 primer. All instruments and materials were obtained from Applied Biosystems unless indicated. The FAM-tagged PCR product (1 μl) together with MegaBAC E^{TM} ET900 (Amersham Bioscience) internal size standard (0.04 μl) were denatured at 94°C, 5 min in 9 μl of HiDi-formamide and analyzed using an ABI3730 sequencer. Data analysis was performed using plate manager application GeneMapper v5.2- 3730XL.

Antibodies

MW8 (26) is a monoclonal antibody that was raised against the peptide AEEPLHRP at the C-terminus of exon 1. MW1 (26) and 3B5H10 (27) (Sigma) are both monoclonal antibodies that detect expanded polyQ tracts, MW1 was raised against polyQ and 3B5H10 (27) was raised against an N-terminal 171 amino acid fragment of huntingtin with 65Q. S830 is a sheep polyclonal antibody that was raised against an exon 1 Htt protein with 53Q (23).

Seprion ligand ELISA

Brains were dissected, snap-frozen in liquid N_2 and stored at −80°C until required. A 2.5% lysate was prepared in ice-cold RIPA buffer (50 mM Tris–HCl pH 8.0; 120 mM NaCl; 1% Igepal; 3.125% sodium deoxycholate; 0.01% SDS; 1 mM β-mercaptoethanol; 1 μM PMSF; 1 mM DTT; protease inhibitor cocktail (Roche)) by ribolysing for 3 × 30 s in Lysing matrix tubes (Lysing matrix D; MP Biomedicals). Samples were stored on ice for 5 min and used immediately or frozen on dry ice, stored at −80°C and used within 24 h. Homogenate (15 μl) was mixed with 3 μl 10% SDS, diluted to 80 μl with water, and then made up to 100 μl with 5× capture buffer (Microsens Biotechnologies). This was transferred to the well of a Seprion ligand-coated ELISA plate, and incubated with shaking for 1 h at room temperature (RT). After removal of the lysate, the well was washed 5× in PBS-T (PBS; 0.1% Tween) and 100 μl S830 primary antibody (diluted 1:2000 in conjugate buffer (150 mM NaCl; 4% BSA (98% electrophoretic grade); 1% non-fat dried milk; 0.1% Tween 20 in PBS) was added and incubated with shaking for 1 h at RT. After five washes with PBS-T, 100 μl horse radish peroxidase (HRP)-conjugated rabbit anti-goat secondary antibody (DAKO) (1:2000 in conjugation buffer) was added and incubated with shaking for 45 min at RT. After washing five times with PBS-T, 100 μl of TMB substrate (SerTec) at RT was added and incubated in the dark (wrapped in foil) at RT for 30 min. Reactions were terminated by the addition of 100 μl 0.5 M HCl and the absorption at 450 nm was measured using a plate reader (Biorad).

Seprion ligand bead capture

A 10% brain homogenate was prepared by ribolysing in ice-cold RIPA buffer for 3 × 30 s in Lysing matrix tubes (Lysing matrix D; MP Biomedicals). Seprion-coated magnetic beads of 100 μl (Microsens Biotechnologies) was transferred to an Eppendorf tube on a magnetic particle concentrator (Dynal MPC-s). The supernatant was removed and replaced with 100 μl of ultrapure water prior to use in the assay. About 50–100 μl of homogenate was diluted to 700 μl with water and made up to 1 ml with 200 μl 5× capture buffer (Microsens Technologies) and 100 μl of coated beads. The tube was shaken on a Vibrax shaker (VXR basic IKA Vibrax) for 1 h at 1000 mot/min at RT, transferred to the magnetic concentrator and the supernatant removed. The beads were washed with 500 μl of 1× capture buffer followed by 2 × 1 ml of TBS (Microsens Biotechnologies) and 1 × 300 μl of TBS. Traces of TBS were removed by pipette after quickly spinning in a microfuge. The captured material was eluted by mixing with 20 μl of 0.75% SDS and heating at 100°C for 5 min in a heating block.

Western blotting

For immunoblotting,10 μl of the eluted material from the bead capture assay was mixed with 5 μl of 2× Laemmli loading buffer, denatured at 100°C for 10 min and loaded on the 10% SDS–PAGE gel. After electrophoresis, proteins were transferred to nitrocellulose membranes (Schleicher and Schuell) in 25 mM Tris–HCl, 192 mM glycine, 20% v/v methanol. Membranes were blocked for overnight in PBS (10 mM Na_2HPO_4, 2 mM KH_2PO_4, 137 mM NaCl, 2.7 mM KCl, (pH7.4)) containing 4% non-fat dried milk at 4°C, washed with PBS-T (PBS with 0.1% tween-20), and incubated for 1 h with the primary antibody (in PBS-T containing 0.5% non-fat dried milk). Blots were washed with PBS-T, probed with HRP-linked secondary antibodies (in PBS with 0.5% non-fat dried milk) for 1 h and washed again with PBS-T. Bound antibodies were visualized using the enhanced chemiluminescence detection system according to the manufacturer's instructions (GE Healthcare). Primary antibodies and dilutions were: S830 (23) (sheep polyclonal Ab 1:750), MW1 (26) (monoclonal Ab 1:1000), MW8 (26) (monoclonal Ab 1:750), 3B5H10 (Sigma) (monoclonal Ab 1:5000), HRP-conjugated secondary antibodies were as follows: rabbit anti-mouse (Dako 1:5000), rabbit anti-goat (Dako, 1:3000). All incubations were performed at RT.

Electron microscopy

For immune-labelling, 20 μl eluted material from the bead capture assay was dried at 95°C in a heating block and resuspended in 9 μl ultrapure water. Three microlitres were transferred to a freshly glow-discharged Formvar/carbon-coated grid and incubated at RT for 1 min. Excess solution was removed and the grid allowed to air-dry for 5 min. Grids were rinsed briefly in PBS and transferred to blocking solution (0.1% BSA-C™ (Aurion) in PBS) for 15 min. This was followed by incubation with primary antibody diluted in blocking solution for 1 h. Antibody dilutions were: MW1 1:100; MW8 1:100; 3B5H10 1:5000. The grids were washed six to eight times in a drop of blocking solution (2 min/drop) and transferred to secondary antibody conjugated with 10 nm colloidal gold particles (BB International) diluted 1:200 in blocking solution for 1 h. The grids were washed as above, followed by two rinses in a drop of ultrapure water (1 min/drop) and air-dried for 3 min. Negative staining was performed by adding 3 μl of 1% uranyl acetate for 45 s, excess stain was removed with hardened filter paper and grids allowed to air-dry. Images were taken with a transmission electron microscope (Tecnai 12 Biotwin; FEI) at 120 kV. For electron tomography, tilt series were acquired fully automatically using FEI proprietary software running on an FEI Tecnai G2 transmission electron microscope operating at 200 kV. Digital images of the structures of interest were recorded at 10 tilt intervals from −650 to +650 on a 2K Gatan Ultrascan CCD camera.

Atomic force microscopy

Aggregates were captured by Seprion beads and eluted with 20 μl 100 mM KCl. From each preparation 2.5 μl was deposited on freshly cleaved mica plate (Ted Pella Inc, Redding, CA) and incubated for 1 min at RT. The captured material was washed with 200 μl of ultrapure water and dried under a gentle stream of air. Exon 1 Htt recombinant proteins (33) were prepared as described in (43) and incubated at a concentration of 20 μM for 1 h. Each deposition was imaged *ex situ* using a MFP3D scanning probe microscope (Asylum Research, Santa Barbara, CA, USA). Images were taken with silicon cantilevers with a nominal spring constant of 40 N/m and resonance frequency of approximately 300 kHz. Typical imaging parameters were: drive amplitude 150–500 mV with set points of 0.7–0.8 V, scan frequencies of 2–4 Hz, image resolution 512 × 512 points, and scan size of 3 μm. All the experiments were performed in duplicates. Several images were obtained from separate locations across the mica surfaces to ensure reproducibility. Quantitative analysis of AFM images: size analysis of aggregates observed by AFM was performed using routines written in MATLAB (MathWorks, Natick, MA, USA) equipped with the image-processing toolbox. Individual aggregates in an AFM image are automatically located and their volumes and heights and other geometrical characteristics are measured, facilitating quick analysis of thousands of individual aggregates. Contributions owing to the finite shape and size of the tip were compensated for, based on geometrical simulations as described previously (44).

Statistical analysis

Statistical analysis was performed by Student's *t*-test and one-way ANOVA using SPSS.

SUPPLEMENTARY MATERIAL

Supplementary Material is available at *HMG* online.

Conflict of Interest statement. The Seprion ligand is provided to us by Microsens Biotechnologies and members of that company are authors on this paper. The R6/2 mice are licensed by King's College London for commercial work.

FUNDING

This work was supported by the Wellcome Trust (66270 to G.P.B.); the Hereditary Disease Foundation (to G.B. and a postdoctoral fellowship to J.L.); Huntington's Disease Society of America Coalition for the Cure (to G.P.B.); the CHDI Foundation (to G.P.B.); the National Institutes of Health (R01 NS047237 to P.J.M., R01 2NS039074 to S.F.); and the Taube-Koret Center for Huntington's Disease Research (to S.F.).

REFERENCES

1. Bates, G.P., Harper, P.S. and Jones, A.L. (2002) *Huntington's Disease*, 3rd edn. Oxford University Press, Oxford, UK.
2. Huntington's Disease Collaborative Research Group. (1993) A novel gene containing a trinucleotide repeat that is expanded and unstable on Huntington's disease chromosomes. *Cell*, **72**, 971–983.
3. DiFiglia, M., Sapp, E., Chase, K.O., Davies, S.W., Bates, G.P., Vonsattel, J.P. and Aronin, N. (1997) Aggregation of huntingtin in neuronal intranuclear inclusions and dystrophic neurites in brain. *Science*, **277**, 1990–1993.
4. Gutekunst, C.A., Li, S.H., Yi, H., Mulroy, J.S., Kuemmerle, S., Jones, R., Rye, D., Ferrante, R.J., Hersch, S.M. and Li, X.J. (1999) Nuclear and neuropil aggregates in Huntington's disease: relationship to neuropathology. *J. Neurosci.*, **19**, 2522–2534.
5. Wacker, J.L., Zareie, M.H., Fong, H., Sarikaya, M. and Muchowski, P.J. (2004) Hsp70 and Hsp40 attenuate formation of spherical and annular polyglutamine oligomers by partitioning monomer. *Nat. Struct. Mol. Biol.*, **11**, 1215–1222.
6. Poirier, M.A., Li, H., Macosko, J., Cai, S., Amzel, M. and Ross, C.A. (2002) Huntingtin spheroids and protofibrils as precursors in polyglutamine fibrilization. *J. Biol. Chem.*, **277**, 41032–41037.
7. Thakur, A.K., Jayaraman, M., Mishra, R., Thakur, M., Chellgren, V.M., Byeon, I.J., Anjum, D.H., Kodali, R., Creamer, T.P., Conway, J.F. *et al.* (2009) Polyglutamine disruption of the huntingtin exon 1 N terminus triggers a complex aggregation mechanism. *Nat. Struct. Mol. Biol.*, **16**, 380–389.
8. Chan, H.Y., Warrick, J.M., Gray-Board, G.L., Paulson, H.L. and Bonini, N.M. (2000) Mechanisms of chaperone suppression of polyglutamine disease: selectivity, synergy and modulation of protein solubility in *Drosophila*. *Hum. Mol. Genet.*, **9**, 2811–2820.
9. Muchowski, P.J., Schaffar, G., Sittler, A., Wanker, E.E., Hayer-Hartl, M.K. and Hartl, F.U. (2000) Hsp70 and hsp40 chaperones can inhibit self-assembly of polyglutamine proteins into amyloid-like fibrils. *Proc. Natl Acad. Sci. USA*, **97**, 7841–7846.
10. Ehrnhoefer, D.E., Duennwald, M., Markovic, P., Wacker, J.L., Engemann, S., Roark, M., Legleiter, J., Marsh, J.L., Thompson, L.M., Lindquist, S. *et al.* (2006) Green tea (-)-epigallocatechin-gallate modulates early events in huntingtin misfolding and reduces toxicity in Huntington's disease models. *Hum. Mol. Genet.*, **15**, 2743–2751.
11. Bodner, R.A., Outeiro, T.F., Altmann, S., Maxwell, M.M., Cho, S.H., Hyman, B.T., McLean, P.J., Young, A.B., Housman, D.E. and Kazantsev, A.G. (2006) Pharmacological promotion of inclusion formation: a therapeutic approach for Huntington's and Parkinson's diseases. *Proc. Natl Acad. Sci. USA*, **103**, 4246–4251.
12. Nekooki-Machida, Y., Kurosawa, M., Nukina, N., Ito, K., Oda, T. and Tanaka, M. (2009) Distinct conformations of *in vitro* and *in vivo* amyloids of huntingtin-exon1 show different cytotoxicity. *Proc. Natl Acad. Sci. USA*, **106**, 9679–9684.
13. Mangiarini, L., Sathasivam, K., Seller, M., Cozens, B., Harper, A., Hetherington, C., Lawton, M., Trottier, Y., Lehrach, H., Davies, S.W. *et al.* (1996) Exon 1 of the HD gene with an expanded CAG repeat is sufficient to cause a progressive neurological phenotype in transgenic mice. *Cell*, **87**, 493–506.
14. Bates, G.P. and Hockly, E. (2003) Experimental therapeutics in Huntington's disease: are models useful for therapeutic trials? *Curr. Opin. Neurol.*, **16**, 465–470.
15. Li, H., Li, S.H., Cheng, A.L., Mangiarini, L., Bates, G.P. and Li, X.J. (1999) Ultrastructural localization and progressive formation of neuropil aggregates in Huntington's disease transgenic mice. *Hum. Mol. Genet.*, **8**, 1227–1236.
16. Smith, D.L., Portier, R., Woodman, B., Hockly, E., Mahal, A., Klunk, W.E., Li, X.J., Wanker, E., Murray, K.D. and Bates, G.P. (2001) Inhibition of polyglutamine aggregation in R6/2 HD brain slices-complex dose-response profiles. *Neurobiol. Dis.*, **8**, 1017–1026.
17. Lin, C.H., Tallaksen-Greene, S., Chien, W.M., Cearley, J.A., Jackson, W.S., Crouse, A.B., Ren, S., Li, X.J., Albin, R.L. and Detloff, P.J. (2001) Neurological abnormalities in a knock-in mouse model of Huntington's disease. *Hum. Mol. Genet.*, **10**, 137–144.
18. Woodman, B., Butler, R., Landles, C., Lupton, M.K., Tse, J., Hockly, E., Moffitt, H., Sathasivam, K. and Bates, G.P. (2007) The Hdh(Q150/Q150) knock-in mouse model of HD and the R6/2 exon 1 model develop comparable and widespread molecular phenotypes. *Brain Res. Bull.*, **72**, 83–97.
19. Kuhn, A., Goldstein, D.R., Hodges, A., Strand, A.D., Sengstag, T., Kooperberg, C., Becanovic, K., Pouladi, M.A., Sathasivam, K., Cha, J.H. *et al.* (2007) Mutant huntingtin's effects on striatal gene expression in mice recapitulate changes observed in human Huntington's disease brain and do not differ with mutant huntingtin length or wild-type huntingtin dosage. *Hum. Mol. Genet.*, **16**, 1845–1861.
20. Davies, S.W., Sathasivam, K., Hobbs, C., Doherty, P., Mangiarini, L., Scherzinger, E., Wanker, E.E. and Bates, G.P. (1999) Detection of polyglutamine aggregation in mouse models. *Methods Enzymol.*, **309**, 687–701.
21. Lane, A., Stanley, C.J., Dealler, S. and Wilson, S.M. (2003) Polymeric ligands with specificity for aggregated prion proteins. *Clin. Chem.*, **49**, 1774–1775.
22. Lane, A.R., Stanley, C.J. and Wilson, S.M. (2003) Binding of pathological forms of prion proteins. Patent PCT/GB03/00858.
23. Sathasivam, K., Woodman, B., Mahal, A., Bertaux, F., Wanker, E.E., Shima, D.T. and Bates, G.P. (2001) Centrosome disorganization in fibroblast cultures derived from R6/2 Huntington's disease (HD) transgenic mice and HD patients. *Hum. Mol. Genet.*, **10**, 2425–2435.
24. Sathasivam, K., Hobbs, C., Turmaine, M., Mangiarini, L., Mahal, A., Bertaux, F., Wanker, E.E., Doherty, P., Davies, S.W. and Bates, G.P. (1999) Formation of polyglutamine inclusions in non-CNS tissue. *Hum. Mol. Genet.*, **8**, 813–822.
25. Hockly, E., Woodman, B., Mahal, A., Lewis, C.M. and Bates, G. (2003) Standardization and statistical approaches to therapeutic trials in the R6/2 mouse. *Brain Res. Bull.*, **61**, 469–479.
26. Ko, J., Ou, S. and Patterson, P.H. (2001) New anti-huntingtin monoclonal antibodies: implications for huntingtin conformation and its binding proteins. *Brain Res. Bull.*, **56**, 319–329.
27. Peters-Libeu, C., Newhouse, Y., Krishnan, P., Cheung, K., Brooks, E., Weisgraber, K. and Finkbeiner, S. (2005) Crystallization and diffraction properties of the Fab fragment of 3B5H10, an antibody specific for disease-causing polyglutamine stretches. *Acta. Crystallogr. Sect. F Struct. Biol. Cryst. Commun.*, **61**, 1065–1068.
28. Yang, W., Dunlap, J.R., Andrews, R.B. and Wetzel, R. (2002) Aggregated polyglutamine peptides delivered to nuclei are toxic to mammalian cells. *Hum. Mol. Genet.*, **11**, 2905–2917.
29. Chen, S., Berthelier, V., Yang, W. and Wetzel, R. (2001) Polyglutamine aggregation behavior in vitro supports a recruitment mechanism of cytotoxicity. *J. Mol. Biol.*, **311**, 173–182.
30. Ehrnhoefer, D.E., Bieschke, J., Boeddrich, A., Herbst, M., Masino, L., Lurz, R., Engemann, S., Pastore, A. and Wanker, E.E. (2008) EGCG redirects amyloidogenic polypeptides into unstructured, off-pathway oligomers. *Nat. Struct. Mol. Biol.*, **15**, 558–566.
31. Dahlgren, P.R., Karymov, M.A., Bankston, J., Holden, T., Thumfort, P., Ingram, V.M. and Lyubchenko, Y.L. (2005) Atomic force microscopy analysis of the Huntington protein nanofibril formation. *Nanomedicine*, **1**, 52–57.
32. Diaz-Hernandez, M., Moreno-Herrero, F., Gomez-Ramos, P., Moran, M.A., Ferrer, I., Baro, A.M., Avila, J., Hernandez, F. and Lucas, J.J. (2004) Biochemical, ultrastructural, and reversibility studies on huntingtin

filaments isolated from mouse and human brain. *J. Neurosci.*, **24**, 9361–9371.
33. Scherzinger, E., Lurz, R., Turmaine, M., Mangiarini, L., Hollenbach, B., Hasenbank, R., Bates, G.P., Davies, S.W., Lehrach, H. and Wanker, E.E. (1997) Huntingtin-encoded polyglutamine expansions form amyloid-like protein aggregates in vitro and in vivo. *Cell*, **90**, 549–558.
34. Scherzinger, E., Sittler, A., Schweiger, K., Heiser, V., Lurz, R., Hasenbank, R., Bates, G.P., Lehrach, H. and Wanker, E.E. (1999) Self-assembly of polyglutamine-containing huntingtin fragments into amyloid-like fibrils: implications for Huntington's disease pathology. *Proc. Natl Acad. Sci. USA*, **96**, 4604–4609.
35. Davies, S.W., Turmaine, M., Cozens, B.A., DiFiglia, M., Sharp, A.H., Ross, C.A., Scherzinger, E., Wanker, E.E., Mangiarini, L. and Bates, G.P. (1997) Formation of neuronal intranuclear inclusions underlies the neurological dysfunction in mice transgenic for the HD mutation. *Cell*, **90**, 537–548.
36. Li, M., Chevalier-Larsen, E.S., Merry, D.E. and Diamond, M.I. (2007) Soluble androgen receptor oligomers underlie pathology in a mouse model of spinobulbar muscular atrophy. *J. Biol. Chem.*, **282**, 3157–3164.
37. Chromy, B.A., Nowak, R.J., Lambert, M.P., Viola, K.L., Chang, L., Velasco, P.T., Jones, B.W., Fernandez, S.J., Lacor, P.N., Horowitz, P. *et al.* (2003) Self-assembly of Abeta(1–42) into globular neurotoxins. *Biochemistry*, **42**, 12749–12760.
38. Kodali, R. and Wetzel, R. (2007) Polymorphism in the intermediates and products of amyloid assembly. *Curr. Opin. Struct. Biol.*, **17**, 48–57.
39. Arimon, M., Diez-Perez, I., Kogan, M.J., Durany, N., Giralt, E., Sanz, F. and Fernandez-Busquets, X. (2005) Fine structure study of Abeta1–42 fibrillogenesis with atomic force microscopy. *FASEB J.*, **19**, 1344–1346.
40. Bennett, M.J., Huey-Tubman, K.E., Herr, A.B., West, A.P. Jr., Ross, S.A. and Bjorkman, P.J. (2002) Inaugural article: a linear lattice model for polyglutamine in CAG-expansion diseases. *Proc. Natl Acad. Sci. USA*, **99**, 11634–11639.
41. Li, P., Huey-Tubman, K.E., Gao, T., Li, X., West, A.P. Jr., Bennett, M.J. and Bjorkman, P.J. (2007) The structure of a polyQ-anti-polyQ complex reveals binding according to a linear lattice model. *Nat. Struct. Mol. Biol.*, **14**, 381–387.
42. Weiss, A., Klein, C., Woodman, B., Sathasivam, K., Bibel, M., Regulier, E., Bates, G.P. and Paganetti, P. (2008) Sensitive biochemical aggregate detection reveals aggregation onset before symptom development in cellular and murine models of Huntington's disease. *J. Neurochem.*, **104**, 846–858.
43. Legleiter, J., Lotz, G.P., Miller, J., Ko, J., Ng, C., Williams, G.L., Finkbeiner, S., Patterson, P.H. and Muchowski, P.J. (2009) Monoclonal antibodies recognize distinct conformational epitopes formed by polyglutamine in a mutant huntingtin fragment. *J. Biol. Chem.*, **284**, 21647–21658.
44. Legleiter, J., Demattos, R., Holtzman, D. and Kowalewski, T. (2004) In situ AFM studies of astrocyte-secreted apolipoprotein E and J-containing lipoproteins. *J. Colloid. Inter. Sci.*, **278**, 96–106.